Title

Enhanced Mandibular Bone Repair by Combined Treatment of Bone Morphogenetic Protein 2 and Small-Molecule Phenamil.

Journal

Tissue engineering. Part A, 23(5-6)

ISSN

1937-3341

Authors

Fan, Jiabing
Guo, Mian
Im, Choong Sung
et al.

Publication Date

2017-03-01

DOI

10.1089/ten.tea.2016.0308

Peer reviewed

TISSUE ENGINEERING: Part A
Volume 23, Numbers 5 and 6, 2017

DOI: 10.1089/ten.tea.2016.0308

termis
Tissue Engineering
& Regenerative Medicine
International Society

ORIGINAL ARTICLE

Enhanced Mandibular Bone Repair by Combined Treatment of Bone Morphogenetic Protein 2 and Small-Molecule Phenamil

Jiabing Fan, MD, PhD,[1] Mian Guo, MD, PhD,[2] Choong Sung Im,[1] Joan Pi-Anfruns, DMD,[3] Zhong-Kai Cui, PhD,[1] Soyon Kim, MS,[4] Benjamin M. Wu, DDS, PhD,[1,4] Tara L. Aghaloo, DDS, MD, PhD,[3,*] and Min Lee, PhD[1,4,*]

Growth factor-based therapeutics using bone morphogenetic protein 2 (BMP-2) presents a promising strategy to reconstruct craniofacial bone defects such as mandible. However, clinical applications require supraphysiological BMP doses that often increase inappropriate adipogenesis, resulting in well-documented, cyst-like bone formation. Here we reported a novel complementary strategy to enhance osteogenesis and mandibular bone repair by using small-molecule phenamil that has been shown to be a strong activator of BMP signaling. Phenamil synergistically induced osteogenic differentiation of human bone marrow mesenchymal stem cells with BMP-2 while suppressing their adipogenic differentiation induced by BMP-2 *in vitro*. The observed pro-osteogenic and antiadipogenic activity of phenamil was mediated by expression of tribbles homolog 3 (Trb3) that enhanced BMP-smad signaling and inhibited expression of peroxisome proliferator-activated receptor gamma (PPARγ), a master regulator of adipogenesis. The synergistic effect of BMP-2+phenamil on bone regeneration was further confirmed in a critical-sized rat mandibular bone defect by implanting polymer scaffolds designed to slowly release the therapeutic molecules. These findings indicate a new complementary osteoinductive strategy to improve clinical efficacy and safety of current BMP-based therapeutics.

Keywords: adipogenesis, BMP-2, hBMSCs, mandible, osteogenesis, phenamil

Introduction

Mandibular defects that often arise from the resection of benign and malignant tumors within the mandible, complications of traumatic injury, or drug/radiation-induced osteonecrosis represent an exclusive challenge to surgical reconstruction.[1,2] The clinical therapeutics using vascularized free flap transfer is currently considered as the gold standard for reconstructing mandibular defects.[3] However, such free tissue transfer may cause donor-site morbidities and requires the lengthy surgery that is often accompanied with high chances of perioperative complications.[4–6] These limitations along with increased clinical exposure to growth factor-mediated therapeutics in craniofacial defects lead to the growing focus on seeking tissue-engineering strategy to augment mandibular repair while minimizing the concerns associated with conventional treatments.[7,8]

One such tissue-engineering approach is to create a bone substitute through incorporating biomaterial scaffolds and exogenous osteoinductive factors such as human recombinant bone morphogenetic protein 2 (BMP-2) that acts as stimuli for the recruitment and differentiation of mesenchymal progenitor cells to neo-bone growth.[9,10] However, the supraphysiological doses of BMP-2 are required to invoke therapeutic response, which cause undesirable adipogenic differentiation rather than osteogenic differentiation, resulting in cyst-like bone formation filled with lipid.[11–14] Moreover, the administration of supraphysiological BMP-2 using an inappropriate delivery system may lead to premature rapid diffusion of BMP-2 out of the defect area, causing ectopic bone formation, tissue inflammation/swelling, or bone resorption.[15–17]

With respect to these highlighted adverse events that impair bone formation in both functionality and aesthetics,

[1]Division of Advanced Prosthodontics, School of Dentistry, University of California, Los Angeles, Los Angeles, California.
[2]Department of Neurosurgery, The 2nd Affiliated Hospital of Harbin Medical University, Harbin, China.
[3]Division of Diagnostic and Surgical Sciences, School of Dentistry, University of California, Los Angeles, Los Angeles, California.
[4]Department of Bioengineering, University of California, Los Angeles, Los Angeles, California.
*Co-senior authors.

there are increasing clinical needs for developing alternative molecular strategies that can effectively complement BMP activity to maximize biological efficiency and simultaneously minimize BMP-induced adipogenesis.[18,19]

We recently reported that phenamil, a derivative of diuretic amiloride, is capable of inducing osteogenesis *in vitro* and *in vivo*.[20,21] Unlike protein-based growth factors, small osteoinductive molecules applied to bone repair exhibit the advantages, including high stability, affordability, and low immunogenicity.[22] The osteogenic competence of phenamil has been evidenced in the elevated osteogenesis of human dental pulp cells, mouse bone marrow stromal or preosteoblastic cells, and mouse adipose-derived stem cells (ASCs), as well as calvarial bone augmentation in mice.[20,23–25]

Moreover, we showed that the osteogenic capacity of phenamil is mediated at least, in part, through induction of tribbles homolog 3 (Trb3) that enhances BMP-smad signaling *via* hindering the expression of Smurf-1, an antagonist of BMP signaling.[20,21] In addition, Trb3 was revealed to inhibit expression of peroxisome proliferator-activated receptor gamma (PPARγ)—a major transcriptional regulator of adipogenesis.[26,27] Together, in addition to its pro-osteogenic property, the small-molecule phenamil is hypothesized to exhibit the inhibitory effect on adipogenic differentiation *via* induction of Trb3.

In this study, we explored a complementary approach to promoting ossification by applying codelivery of BMP-2 and phenamil to mandibular bone defects. First, the human bone marrow mesenchymal stem cells (hBMSCs) were utilized to study combined effects of BMP-2 and phenamil on osteogenic/adipogenic differentiation *in vitro*. Second, a biomimetic apatite-coated poly(lactic-co-glycolic acid) (PLGA) scaffold, which was previously well studied to enhance osteogenesis of progenitor cells as well as sustained release of the loaded osteoinductive factors,[28,29] was used to codeliver BMP-2 and phenamil. The three-dimensional (3D) construct was further implanted into a 5-mm critical-sized mandible defect created in rat to investigate their osteogenic capacity *in vivo*. Overall, these studies provide a potent complementary therapy adopting BMP-2 and phenamil for mandibular bone treatment.

Materials and Methods

hBMSC culture

hMSCs ($n=2$ patients) were purchased from Lonza (Vancouver, Canada) and grown in the human MesenCult™ proliferation medium (STEMCELL Technologies). The amplified cells at passage 2 were used for further experiments.

Alkaline phosphatase activity and Alizarin red staining

To induce osteogenic differentiation, hBMSCs were seeded on the 12-well plate and cultured in the growth medium. When the cells reached ~100% confluence, the culture medium was replaced by differentiation-inducing medium consisting of 50 μg/mL L-ascorbic acid (Sigma), 10 mM β-glycerophosphate (Sigma), and 100 nM dexamethasone (Sigma), in the presence or absence of BMP-2 (100 ng/mL) and/or phenamil (20 μM). To detect alkaline phosphatase (ALP) expression, the cells were induced for 3 days, fixed with 10% formalin (Sigma), stained with ALP kit containing AP buffer (100 mM Tris pH 8.5, 50 mM $MgCl_2$, 100 mM NaCl) supplemented with nitroblue tetrazolium (NBT; Sigma) and 5-Bromo-4-chloro-3-indolyl phosphate (BCIP; Sigma) stock solutions as described previously, and imaged with the Olympus BX51 microscope.

Each image of ALP staining was further quantified by ImageJ software (NIH). For the colorimetric measurement of ALP activity, the cells were dissolved in 0.2% NP-40 lysis buffer (Life Technologies) followed by adding p-nitrophenol phosphate substrate (Sigma) into the buffer, and assessed by absorbance measurement at 405 nm in a multiplate reader. Each measurement was eventually normalized using total DNA content measured by the PicoGreen dsDNA Assay (Life Technologies).

Alizarin red staining was used to detect calcium deposition following the protocol described previously.[30] After 3 weeks of differentiation, the cells were fixed in 10% formalin and stained with 2% Alizarin red solution (Sigma) for 5 min. The stained samples were washed in ddH_2O up to three times and imaged with the Olympus BX51 microscope. To quantify mineralization, the stained cells were dissolved in 10% (v/v) acetic acid and the absorbance was measured at 405 nm.

AdipoRed assay and Oil red staining

To induce adipogenic differentiation, the cells growing in 12-well plate were incubated in human MesenCult adipogenic medium after reaching ~100% confluence. After 7 days of incubation, intracellular lipid accumulation derived from differentiated adipocytes was evaluated by the AdipoRed Kit (Lonza) using absorbance at 572 nm. After 2 weeks, the induced cells were fixed with 10% formalin (Sigma), stained with Oil red O solution (Sigma) for 15 min, and imaged with Olympus BX51 microscope. Each staining image was further quantified by ImageJ software (NIH).

RNA extraction and quantitative real-time polymerase chain reaction

Total RNA extraction from hBMSCs was performed by using the TRIzol reagent (Life Technologies) and RNeasy Mini kit (Qiagen) according to the manufacturer's protocol. Complementary DNA was synthesized from 500 ng aliquots of RNA, using a SuperScript III First-Strand Synthesis System (Life Technologies) following the manufacturer's instructions. Quantitative real-time polymerase chain reaction (qRT-PCR) analysis was performed on a 20 μL of SYBR Green reaction system in LightCycler 480 PCR instrument (Roche). Measured *GAPDH* expression level was used in normalizing expression levels of target genes. The sequences for each primer are presented in Supplementary Table S1 (Supplementary Data are available online at www.liebertpub.com/tea).

Western blot assay

The western blot assay was carried out according to previous methods described.[21] In general, the cells were lysed in 0.2% NP-40 lysis buffer (Life Technologies). The protein concentration was measured using a bicinchoninic acid (BCA) protein assay (Thermo Scientific). The

protein lysates were separated by sodium dodecyl sulfate–polyacrylamide gel electrophoresis and blotted onto Immobilon polyvinylidene difluoride (PVDF) membrane (Millipore, Billerica, MA). The primary antibodies used for immunodetection were anti-Trb3 (Santa Cruz), anti-PPARγ (Santa Cruz), anti-Smurf-1, anti-pSmad1/5/8 (Santa Cruz), and anti-GAPDH (Santa Cruz). After the membranes were incubated in the horseradish peroxidase (HRP)-conjugated secondary antibody (Millipore) for 1 h, the immunoreactive complexes were subsequently detected using chemiluminescent HRP (Denville Scientific).

Luciferase assay

Id1 luciferase reporter assay was performed according to the manufacturer's instructions. Briefly, when the cells reached 70–80% confluence, they were cotransfected with pGL4[luc2P/hID1/Hygro] Vector (Promega) and Renilla control vector (Promega) using Lipofectamine 2000 (Life Technologies). After 6 h, the transfection medium was changed to a growth medium in the presence and absence of BMP-2 (100 ng/mL) or/and phenamil (20 μM). After 48 h of treatment, luciferase activities were analyzed using a dual-luciferase reporter system (Promega) and normalized with Renilla internal control values.

Preparation of scaffold

Apatite-coated PLGA (Ap-PLGA) scaffolds were fabricated by solvent casting and particulate leaching process as previously described.[31,32] Briefly, PLGA/chloroform solution was mixed with sucrose (200–300 μm diameter) to achieve a porosity of 92% (volume fraction) and compressed into Teflon molds. After being freeze-dried overnight at 100 mTorr and −110°C (SP Industries, Inc.), the scaffolds were subsequently immersed in double-distilled (dd) H_2O to wash away sucrose. The scaffolds were then disinfected in 70% ethanol for 30 min, followed by rinse in sterile ddH_2O. Finally, the scaffold sheets were cut into $5\times5\times2$ mm plates. The PLGA scaffolds were further coated with apatite layer by incubating scaffolds in simulated body fluid (SBF) according to previous methods described.

The scaffold plates were subjected to glow discharge argon plasma etching (Harrick Scientific, Pleasantville, NY). The etched scaffolds were incubated in SBF1 formulated by dissolving $CaCl_2$, $MgCl_2\cdot6H_2O$, $NaHCO_3$, $K_2HPO_4\cdot3H_2O$, Na_2SO_4, KCl, and NaCl for 24 h and then further incubated in SBF2 formulated by dissolving $CaCl_2$, $K_2HPO_4\cdot3H_2O$, KCl, and NaCl for another 24 h at 37°C. The apatite-coated PLGA scaffolds were loaded with phosphate-buffered saline (PBS), BMP-2, and/or phenamil and were lyophilized for further experiments.

Mandible defect model

Animal usage in these studies was performed according to the protocols set up by the UCLA Animal Research Committee and was in compliance with the Guidelines for the Care and Use of Laboratory Animal of the National Institutes of Health.

The critical-sized mandible defects (5×5 mm) in Sprague Dawley rats (Charles River) at the age of 8–12 weeks were created according to procedures designed previously.[33] Animals were divided into six experimental groups (one defect per animal) according to the implant contents as specified in Table 1. Animals underwent general anesthesia using inhalational isoflurane. The animals were shaved on the ventral surface of mandible, then prepped, and draped in a sterile manner. An incision that overlies and parallels the left mandible was made by a size No. 15 blade. The inferior border of the mandible was then identified when continuing to deepen down through subcutaneous tissues. The mandible body was exposed after separating the pterygomasseteric sling using electrocautery, and the lingual and buccal surfaces of the mandible were further exposed with supraperiosteal lifting of the musculature.

A 1-mm high-speed cutting burr (3000 rpm) was adopted to drill a defect with constant copious irrigation. Hemostasis was then attained with electrocautery and the wound was irrigated to remove bone dust. The appropriate size scaffold with loaded drug was then placed onto the mandibular defect with a resorbable suture, followed by skin closure with nonresorbable suture. All surgical animals were allowed to recover from anesthesia on warm sheet and then transferred to the vivarium for postoperative care. Postoperatively, all animals attained analgesia by subcutaneous injections of buprenorphine (0.1 mg/kg) for 3 days and received trimethoprim–sulfamethoxazole contained in the drinking water supply for 7 days against potential infection. Animals were sacrificed at 10 days and 8 weeks postoperation depending on experimental group assignment.

Microcomputerized tomography scanning

Animals were sacrificed at 8 weeks postimplantation. Left hemimandible tissues were harvested and fixed in 4% formaldehyde at room temperature with gentle shaking for 48 h. The fixed samples were then rinsed with PBS and stored in 70% ethanol before being imaged using the high-resolution microcomputerized tomography (μCT) machine (μCT SkyScan 1172; SkyScan, Kontich, Belgium) set at 57 kVp, 184 μA, 0.5 mm aluminum filtration, and 10 μm resolution.

All data were visualized and reconstructed using Dolphin 3D software (Dolphin Imaging & Management Solutions, Chatsworth, CA). The volume and area of new bone were measured using CTAn (SkyScan) and ImageJ software (NIH), respectively. Bone-specific analysis included new bone area/original defect area (percent area), new bone volume/total volume (percent BV/TV), and trabecular number (TN; mm^{-1}). The TV was termed as the bone volume of the original surgical defect that measured $5\times5\times2.5$ mm.

Table 1. List of Experimental Groups

Group	*No. of animals (10 days)*	*No. of animals (8 weeks)*
Blank	3	5
BMP (1.25 μg)	0	5
BMP (2.5 μg)	3	5
Phe (300 μM)	3	5
BMP (1.25 μg)+Phe (300 μM)	0	5
BMP (2.5 μg)+Phe (300 μM)	3	5

BMP, bone morphogenetic protein; Phe, phenamil.

Histological and immunohistochemical analyses

The fixed mandible tissues were decalcified in 10% ethylenediaminetetraacetic acid (EDTA) solution with gentle shaking for 2 weeks. Decalcified tissues were embedded in paraffin and cut into 5 μm thickness of sections. The tissue sections were deparaffinized with xylene and stained with hematoxylin and eosin (H&E) solution. The deparaffinized sections were further stained with 0.1% Picrosirius red solution (Polysciences, Inc.) and imaged under polarizing light microscope. Masson's trichrome staining kit (Sigma) was also applied to the detection of new bone formation indicated with light blue color.

Additional sections were undergone by immunohistochemical analysis. The deparaffinized sections were treated using citric acid antigen retrieval, incubated with the primary antibodies (Santa Cruz), including anti-Trb3, Smurf-1, pSmad1/5/8, Runx-2, osteocalcin (OCN), and were stained by the HRP/DAB detection kit (Abcam) according to the manufacturer's instructions. The sections were further counterstained with Mayer's hematoxylin (Abcam). Each stained image was further quantified by ImageJ software (NIH).

Statistical analysis

Statistical analysis was conducted by one-way analysis of variance, with the Tukey's *post hoc* test, as more than two groups were compared. Student's *t*-test was implemented to compare two groups. The data are presented as mean ± standard deviation. A p-value of <0.05 was considered statistically significant.

Results

Synergistic effect of BMP-2+phenamil on osteogenic differentiation of hBMSCs via BMP signaling

The prior studies showed that small-molecule phenamil dose dependently induced osteogenic differentiation in mASCs up to 20 μM.[20] To further examine the combined effect of BMP-2+phenamil on osteogenic differentiation of MSCs, we treated hBMSCs with BMP-2 (100 ng/mL) or/and phenamil (20 μM). As evidenced by ALP staining and activity, the expression of ALP, an early osteogenic marker, was increased up to 4.8-fold by either BMP-2 or phenamil treatment, compared with controls, while a synergistic 9.3-fold increase was attained in the combination of BMP-2+phenamil after 3 days of culture (Fig. 1A, B).

By using qRT-PCR analysis, we evaluated the expression of osteogenic gene markers, including *Runx2*, *Osterix*, *ALP*, and *OCN* in hBMSCs, on day 3 of culture. Treatment with BMP-2 alone increased the level of *Runx2* and *Osterix* (critical osteogenic transcription genes) to 2.5- and 18.9-fold, respectively. By simultaneous stimulation with phenamil and BMP-2, the expressions of *Runx2* and *Osterix* significantly increased up to 4.9-fold and 32.7-fold, respectively, compared with nontreated control groups (Fig. 1C). In addition, hBMSCs treated with both BMP-2 and phenamil showed higher *ALP* expression than those individually treated with BMP-2 or phenamil alone, thereby further confirming the above results of ALP staining and activity (Fig. 1C).

Further observation on *OCN* expression revealed a 2.1-fold increase in the hBMSCs treated with BMP-2 alone, followed by phenamil supplemented, resulting in a 2.8-fold increase (Fig. 1C). Finally, the end-stage osteogenesis was evaluated by assessing extracellular matrix mineralization through Alizarin red staining and quantitation on day 21 (Fig. 1D, E). A synergistic increase up to eightfold was detected in the hBMSCs with combinatorial treatment compared with the controls, while BMP-2 or phenamil alone only increased the level of mineral expression to 3.5- and 2.6-fold, respectively (Fig. 1D, E). Collectively, the results indicated that the treatment of BMP-2+phenamil acted synergistically to promote osteogenic differentiation in hBMSCs *in vitro*.

We previously reported that phenamil-induced osteogenesis is mainly mediated through expression of Trb3, which can enhance BMP signaling.[21] To elucidate whether the enhanced osteogenesis by BMP-2+phenamil is regulated by BMP-smad signaling, we performed western blot assay to assess pSmad1/5/8 and Trb3 expression in hBMSCs at day 2. The results confirmed that the treatment of phenamil independent of BMP-2 increased Trb3 expression, whereas the upregulation of Trb3 further increased pSmad 1/5/8 expression by inhibiting Smurf-1 expression, a BMP signaling antagonist (Fig. 1F).

A higher expression of pSmad1/5/8 was observed in hBMSCs treated with BMP-2+phenamil in comparison with other groups. Since Id1 is one of the major downstream targets of BMP signaling, we further monitored the activity of Id1 in hBMSCs at day 2 using luciferase reporter assay. Compared with controls, BMP-2 treatment increased the Id1 luciferase activity by 2.16-fold, with the increased level comparable to phenamil treatment (Fig. 1G). By simultaneous stimulation with phenamil and BMP-2, the Id1 activity increased up to 4.2-fold, which further validated the enhanced BMP-smad pathway observed above.

Phenamil inhibits BMP-2-induced adipogenesis in hBMSCs via PPARγ

In addition to its osteogenic effect, BMP-2 is known to promote adipogenic differentiation that may be associated with the complications occurring during bone repair.[14] To investigate whether phenamil inhibits BMP-2-induced adipogenic differentiation of MSCs, we continued to treat hBMSCs with adipogenic medium supplemented with phenamil and/or BMP-2. qRT-PCR analysis revealed that treatment of BMP-2 at the concentration of 300 ng/mL significantly increased *PPARγ* expression (a major adipogenic transcriptional gene) by 9.7-fold, as well as *LPL* and *adiponectin* (both mature adipogenic genes) expression by 2.1-fold and 2.2-fold, respectively, compared with the controls after 3 days (Fig. 2A). In contrast, addition of phenamil at 10 μM was shown to decrease 2-fold of *PPARγ* expression, 2.1-fold of *LPL* expression, and 1.7-fold of *adiponectin* expression induced by BMP-2 (Fig. 2A).

Furthermore, accumulation of lipid, a major cellular matrix of adipocytes, was detected by Oil red staining and AdipoRed assay (Fig. 2B, C). When compared with controls, BMP-2- treated hBMSCs increased lipid accumulation to 1.5-fold at day 7, while phenamil treatment significantly reduced the expression level, which is consistent with the Oil red staining (Fig. 2B, C). Together, these data demonstrated that phenamil is able to inhibit high-dosage BMP-2-induced adipogenesis in hBMSCs.

To further understand the role of Trb3 in phenamil-mediated suppression on adipogenesis, Trb3 expression at gene and protein level was assessed in hBMSCs at day 3 by qRT-PCR and western blot analysis, respectively. The results showed that

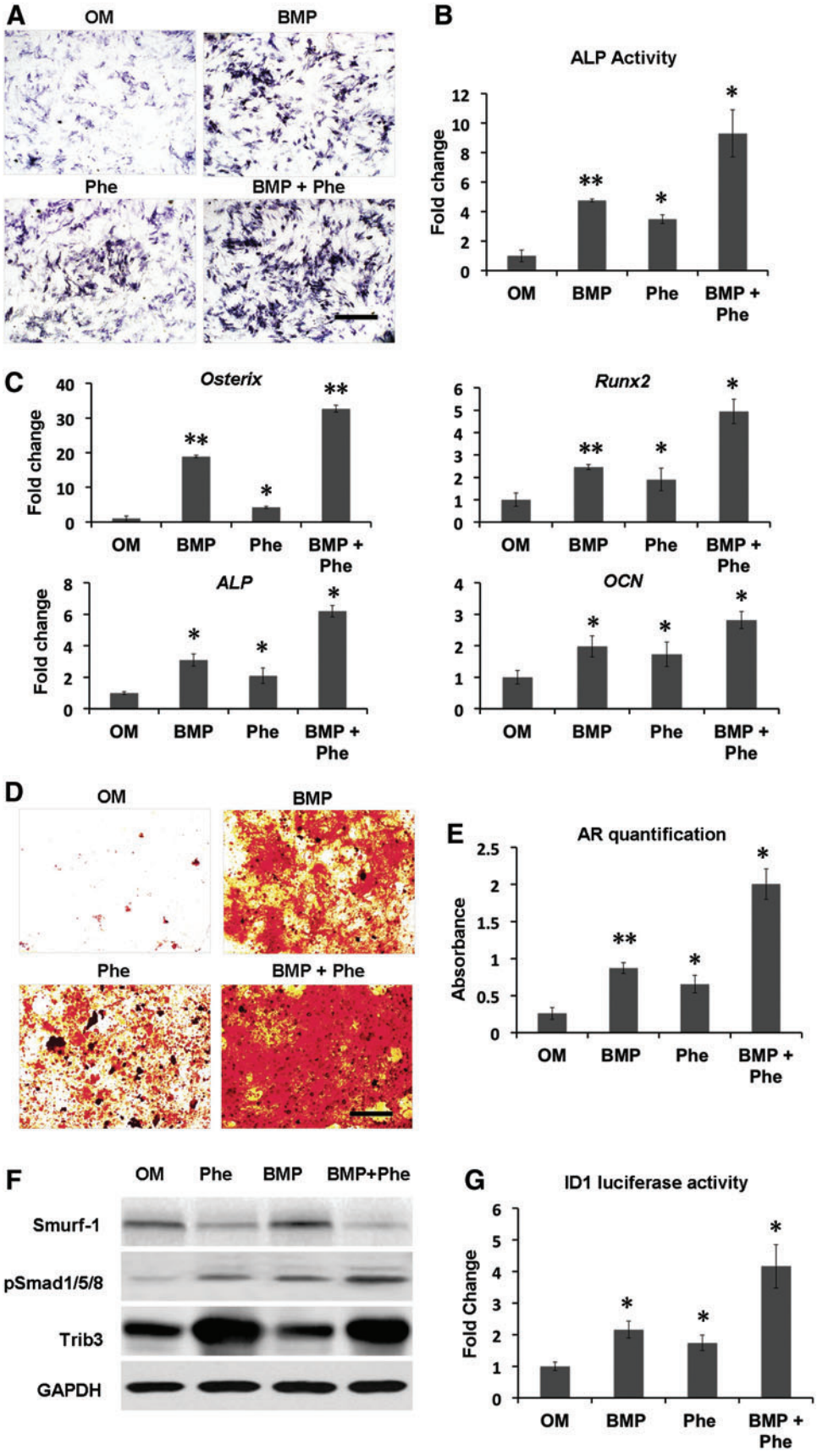

FIG. 1. Combinatorial treatment using BMP-2 and phenamil enhances osteogenic differentiation of hBMSCs in monolayer culture through regulating BMP signaling. Osteogenic markers and BMP signaling were, respectively, measured in hBMSCs treated with BMP-2 100 ng/mL, or phenamil 20 μM, or combination. **(A, B)** ALP expression was assessed by ALP staining and activity at day 3. Scale bar = 500 μm. **(C)** The upregulated expression of osteogenic genes, including *Runx2*, *Osterix*, *ALP*, and *OCN*, was noted in the hBMSCs in the presence of BMP-2 and phenamil, as analyzed by real-time PCR at day 3. **(D, E)** The expression of extracellular matrix mineralization increased in hBMSCs treated with OM in the presence of BMP-2 and phenamil as measured by AR staining and quantification at day 21. Scale bar = 500 μm. **(F)** hBMSCs treated with BMP-2+phenamil revealed the enhanced BMP-smad signaling pathway as evaluated by western blot assay at day 2. Phenamil treatment is able to trigger Trb3 expression that further prohibits Smurf1 (BMP antagonist) to stabilize pSmad 1/5/8. **(G)** Id1 activity was measured by luciferase assay at day 2. Data presented as mean ± SD ($n = 3$/group), $*p < 0.05$, $**p < 0.01$ versus OM. ALP, alkaline phosphatase; AR, Alizarin red staining; BMP-2, bone morphogenetic protein 2; hBMSCs, human bone marrow mesenchymal stem cells; OCN, osteocalcin; OM, osteogenic medium; PCR, polymerase chain reaction; Phe, phenamil; SD, standard deviation; Trb3, tribbles homolog 3. Color images available online at www.liebertpub.com/tea

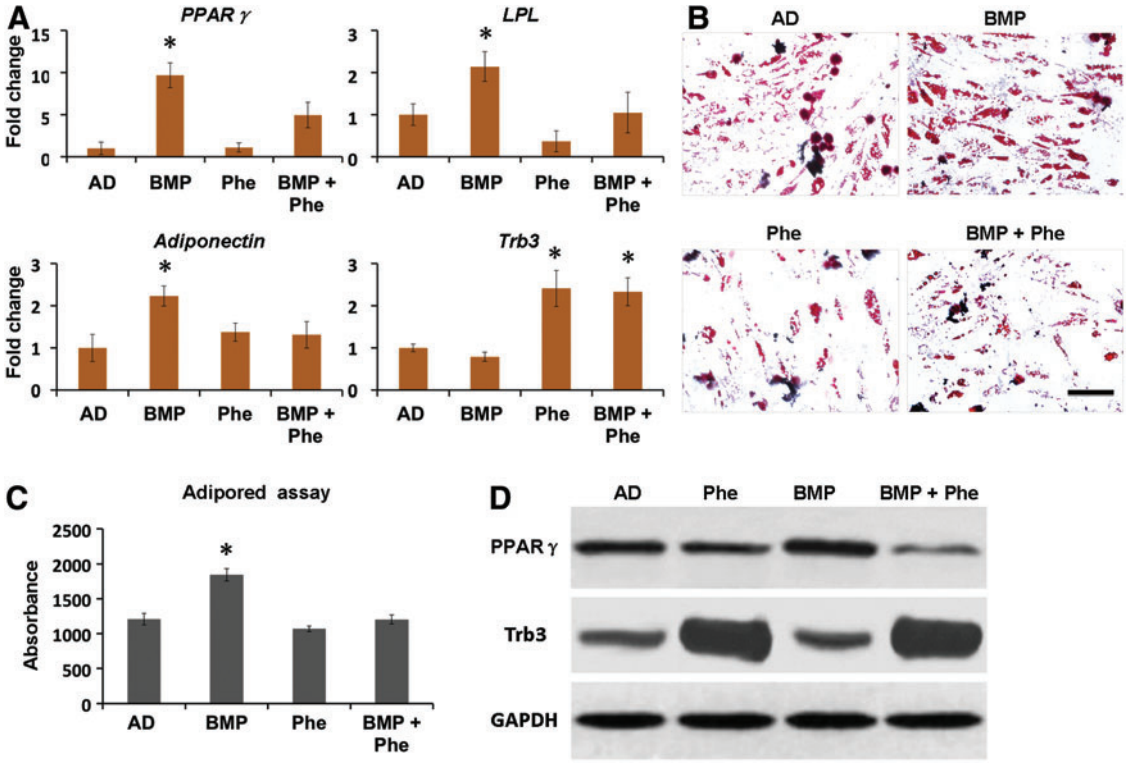

FIG. 2. Phenamil treatment exerts the inhibitory effect on the adipogenic differentiation of hBMSCs by prohibition of PPARγ. To measure their adipogenic differentiation, hBMSCs were cultured with AD supplemented with BMP-2 300 ng/mL, or phenamil 10 μM, or both. **(A)** Adipogenic gene expression, including *PPARγ*, *Adiponectin*, and *LPL*, was measured by real-time PCR assay at day 3. **(B, C)** Lipid accumulation was assessed by OR staining at day 14 and AdipoRed assay at day 7. **(D)** Phenamil prohibits adipogenesis by induction of Trb3 that negatively regulates PPARγ expression as analyzed by western blot assay at day 3. Scale bar = 500 μm. Data presented as mean ± SD ($n = 3$/group), $*p < 0.05$ versus AD. AD, adipogenic differentiation; OR, Oil red staining; PPARγ, peroxisome proliferator-activated receptor gamma. Color images available online at www.liebertpub.com/tea

Trb3 expression in the hBMSCs treated with phenamil in the presence or absence of BMP-2 is higher than that in the hBMSCs treated without phenamil (Fig. 2A, D). The detected Trb3 was accompanied by the reduction of PPARγ expression induced by BMP-2 (Fig. 2D), suggesting that the critical role of Trb3 in phenamil inhibited PPARγ expression and adipogenic differentiation.

BMP signaling and osteogenesis enhanced by BMP-2 and phenamil in vivo

To examine the combined effect on BMP signaling and osteogenesis *in vivo*, apatite-coated PLGA scaffolds were fabricated to deliver BMP-2 and/or phenamil and further implanted into mandibular defects created in rat mandible. We elected the apatite-coated PLGA scaffold as a delivery vehicle due to the capability of the scaffold in maintaining loaded molecules with high stability as well as sustainability.[21]

First, 10 days postoperatively, there was no obvious bone formation observed among the experimental groups as shown in H&E staining (Fig. 3A). As detected by immunohistochemical staining, higher expression of Trb3 was observed in defects treated with the scaffold loaded with phenamil (300 μM) in the presence and absence of BMP-2 (2.5 μg) compared with the defect implanted with blank scaffold (Fig. 3B, D). Furthermore, Smurf-1 expression in the phenamil-treated defects in the presence and absence of BMP was significantly lower than that of blank scaffold-treated defects, while there is no significant difference between BMP-2-alone and control groups (Fig. 3C, E). Finally, treatment of BMP-2 or phenamil was found to increase BMP-smad signaling as determined with pSmad1/5/8 staining in the defects.

When compared with the groups treated with either BMP-2 or phenamil alone, the higher expression of pSmad1/5/8 was observed in the defects treated with both BMP-2 and phenamil, with ~1.5-fold increase as determined by semi-quantitation of immunohistochemical staining (Fig. 3D, G). The enhanced BMP activity was subsequently evidenced to lead to enhanced osteogenesis in defects as stained by osteogenic markers, including Runx2 and OCN (Fig. 4A, B). Semiquantification of the immunohistochemical staining revealed that groups treated with scaffolds releasing both phenamil and BMP-2 exhibited the most intense Runx2 and OCN expression than other groups (Fig. 4C, D). Collectively, the enhanced osteogenesis by codelivery of BMP-2+phenamil *in vivo* might be due to the upregulated BMP/smad signaling, with these results being consistent with *in vitro* findings.

Synergistic increase of mandibular bone formation by BMP-2 and phenamil

To further evaluate the combined effect of BMP-2+phenamil on bone regeneration in a mandibular defect

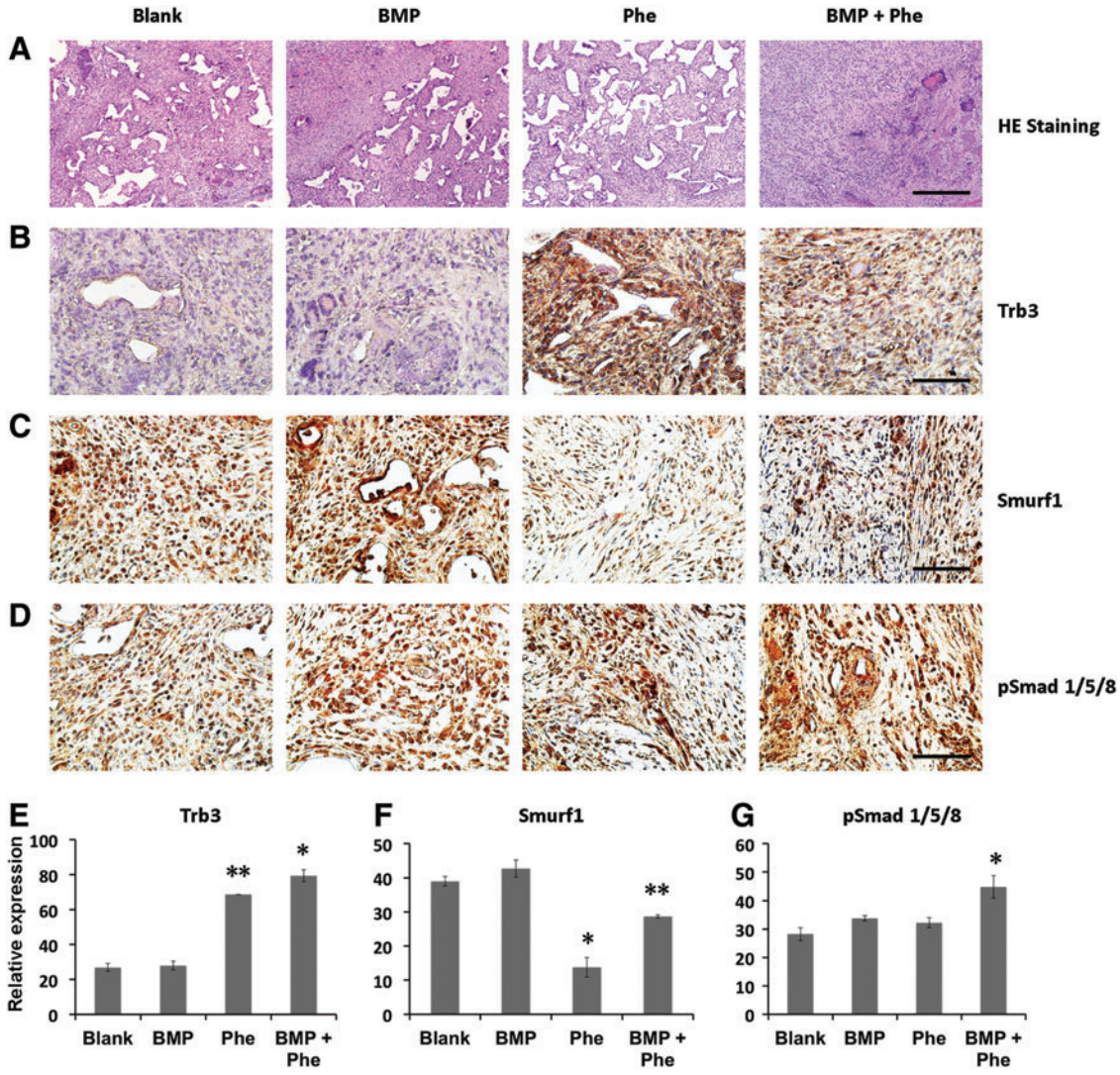

FIG. 3. BMP-2+phenamil treating mandible defects showed the upregulated BMP-smad signaling at 10 days postoperatively. **(A)** Histological staining of mandible defects treated with Ap-PLGA scaffolds loaded with blank, BMP-2 (2.5 μg), phenamil (300 μM), or BMP-2 (2.5 μg) + phenamil (300 μM). Images were taken at 10× magnification. Scale bar = 200 μm. **(B–D)** The expression of Trb3, Smurf-1, and pSmad1/5/8 was, respectively, measured by immunohistochemical staining. **(E–G)** Semi-quantitative analysis of Trb3, Smurf-1, and pSmad1/5/8 staining using ImageJ software. Images were taken at 40× magnification. Scale bar = 50 μm. Data presented as mean ± SD. $*p < 0.05$, $**p < 0.01$. Ap-PLGA, Apatite-coated poly(lactic-co-glycolic acid). Color images available online at www.liebertpub.com/tea

model, we created a critical-sized (5 × 5 mm) mandibular defect in rat mandible and implanted Ap-PLGA scaffolds loaded with BMP-2 or/and phenamil. Over an 8-week postoperative period, all animals remained healthy without obvious infection. By gross observation of the harvested tissues after 8 weeks operatively, defects treated with BMP-2+phenamil restored the native mandibular contour with good integration with the surrounding mandible, but incomplete mandibular restoration was observed in the defect treated with BMP-2 or phenamil alone as well as blank scaffolds (Fig. 5A).

Next, μCT imaging revealed that BMP-2 induced bone formation in mandibular defects (Fig. 5B). Bone formation was evident in the defects treated with 1.25 μg BMP-2. Although treatment of defects with twofold more BMP-2 (2.5 μg) significantly increased bone formation, there was still no complete bone healing found. In contrast, the addition of phenamil at 300 μM synergistically augmented bone healing with BMP-2 as observed by an intensive bone matrix filled in the defect (Fig. 5B). Notably, the defects treated with 2.5 μg BMP-2+phenamil resulted in almost complete bone healing comparable to native mandibular bone (Fig. 5B).

Finally, new bone area, bone volume fraction (BV/TV), and TN were examined to quantitatively analyze the extent of bone repair within the mandibular defects. The results revealed that defects treated with BMP-2 alone increased bone healing, amounting to 55–90% and 22–40% by new bone areas (Fig. 5C) and volume (Fig. 5D), respectively. In contrast, the treatment of defects with both BMP-2 (2.5 μg) and phenamil showed a striking increase in bone healing, ~98.1% and 96% by new bone areas and volume, respectively. Likewise, a higher TN was also detected in the defects

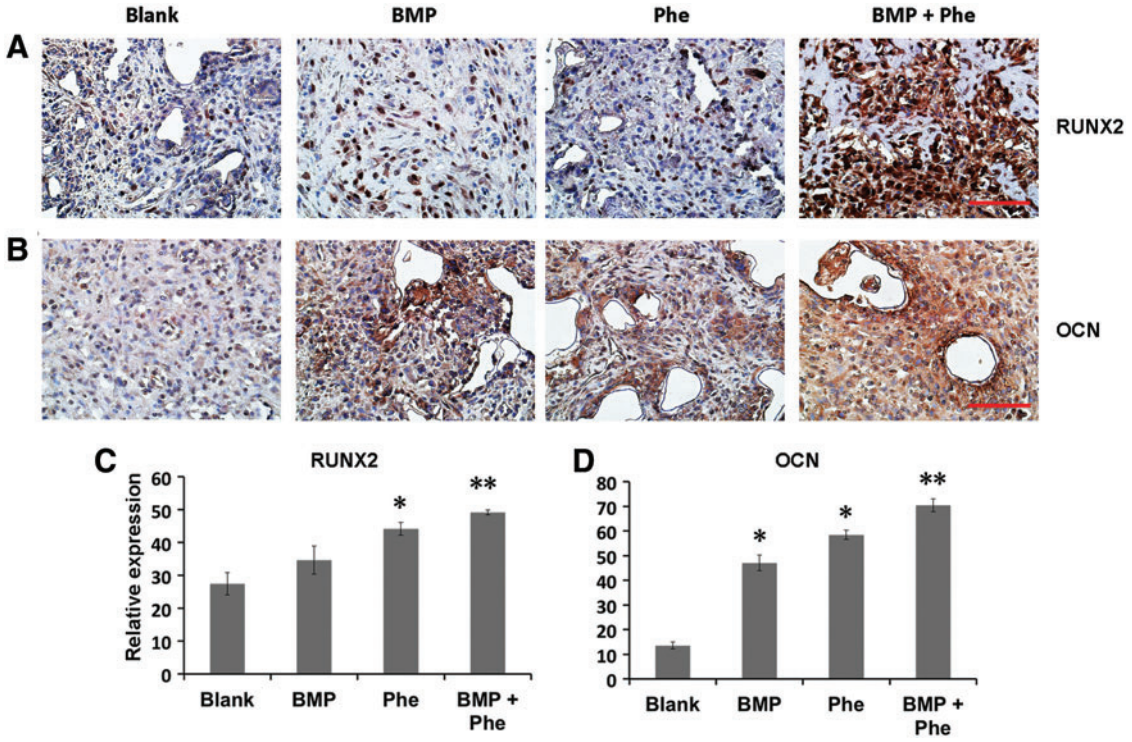

FIG. 4. The mandibular defects treated with both BMP-2 (2.5 μg) and phenamil (300 μM) revealed the enhanced expression of osteogenic markers as early as 10 days postoperatively. **(A, B)** Runx2 and OCN were, respectively, assessed with immunohistochemical staining. **(C, D)** Semiquantitative analysis of Runx2 and OCN staining using ImageJ software. Images were taken at 40× magnification. Scale bar = 50 μm. Data presented as mean ± SD ($n = 3$/group). $*p < 0.05$, $**p < 0.01$. Color images available online at www.liebertpub.com/tea

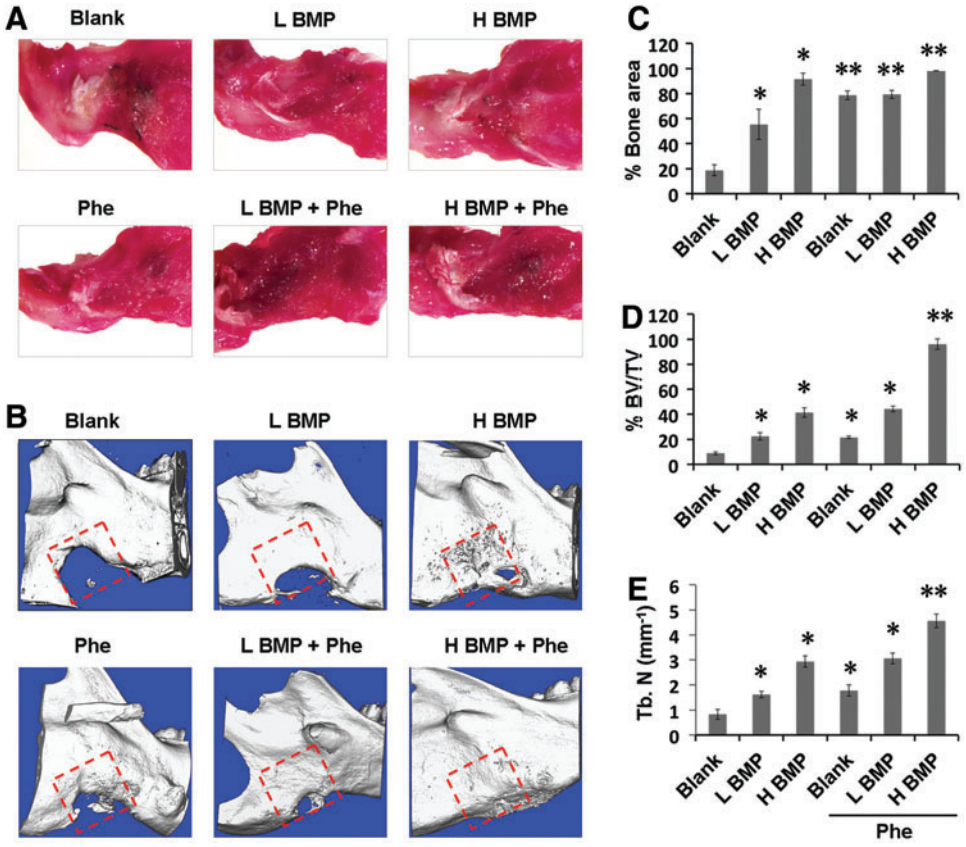

FIG. 5. Codelivery of BMP-2 and phenamil using Ap-PLGA scaffold synergistically acts as bone repair in a critical-sized (5 × 5 mm) mandibular defect created in rat at 8 weeks postoperatively. **(A)** Raw mandible tissues were extracted from rat mandible. **(B)** μCT images of mandibular defects treated with Ap-PLGA scaffolds loaded with BMP-2 and phenamil. *Red square* indicates the original defect. Quantification of percent bone surface area **(C)**, percent BV/TV **(D)**, and TN (mm^{-1}) **(E)**. Data presented as mean ± SD ($n = 5$/group), $*p < 0.05$, $**p < 0.01$ versus blank scaffold. μCT, microcomputerized tomography; BV/TV, bone volume/total volume; H BMP, high-dose BMP-2 (2.5 μg); L BMP, low-dose BMP-2 (1.25 μg); Phe, phenamil (300 μM); TN, trabecular number. Color images available online at www.liebertpub.com/tea

treated with BMP-2 at 2.5 μg + phenamil than any other treatment groups (Fig. 5E).

Histological and immunohistochemical analysis of mandibular bone repair by BMP-2 and phenamil

We then adopted histological evaluation to confirm neobone formation detected in μCT imaging. H&E staining exhibited large matured bone formation as well as osteoid matrix completely spanning and bridging the mandibular defect area when treated with BMP-2 (1.25 or 2.5 μg) + phenamil 300 μM after 8 weeks (Fig. 6A, B). In contrast, insufficient ossification was detected in the defects treated with BMP-2 or phenamil alone (Fig. 6A, B). As analyzed by Masson's trichrome staining, a larger amount of trabecular bone formation appeared throughout the defects treated with both BMP-2 and phenamil, confirming the regenerated bone tissue detected by H&E staining (Fig. 6C).

To further assess the quality of bone healing, the organization and distribution of collagen in the mandibular defect area were also detected by Picrosirius red staining with polarized light microscopy. Highly intense and mixed birefringence of collagen was observed in the defects treated with BMP-2+phenamil compared with the other groups. Moreover, organization of these collagen fibers is shown to be similar to that of collagen fibers observed in native mandible bones (Fig. 6D).

In addition, immunohistochemical staining demonstrated that the defects treated with BMP-2+phenamil revealed higher expression of OCN, a protein that is associated with bone matrix mineralization, compared with other groups (Fig. 7A, D). Notably, the defects treated with low-dose BMP-2 at 1.25 μg and phenamil at 300 μM revealed higher OCN expression in bone healing area compared with groups treated with BMP-2 or phenamil alone. In addition, the high expression of PPARγ was found only in the defect treated with BMP-2 at 2.5 μg (Fig. 7B, E). In contrast, phenamil-treated defects with or without BMP-2 revealed no significant PPARγ expression (Fig. 7B, E). Similarly, the osteoclast cells were only detected in the 2.5 μg BMP-2-treated defects as demonstrated by tartrate-resistant acid phosphatase staining (Fig. 7C).

Discussion

The growth factor-mediated tissue engineering strategy holds promise in the therapeutics of craniofacial bone defects, especially for large mandible deficiency.[34] However, there are several obstacles still prohibiting the wide use of growth factor-based therapeutics clinically and commercially.[35] One major barrier in the adoption of single growth factor BMP-2 is the requirement of supraphysiological therapeutic dosage, which may lead to worrisome complications and high medical burden.[13] In previous studies, up to 10 μg BMP-2 was applied to the treatment of rat mandibular bone defect with a diameter of 2–5 mm, showing around 30% bone healing during 4–8 weeks postsurgery,[36,37] whereas a higher dosage of 1 mg BMP-2 treating a primate mandibular defect with a 20 mm diameter only displayed a slight bone formation at 16 weeks.[9]

The present studies demonstrated that <1.3 μg BMP-2 combined with 300 μM phenamil exerts a striking bone

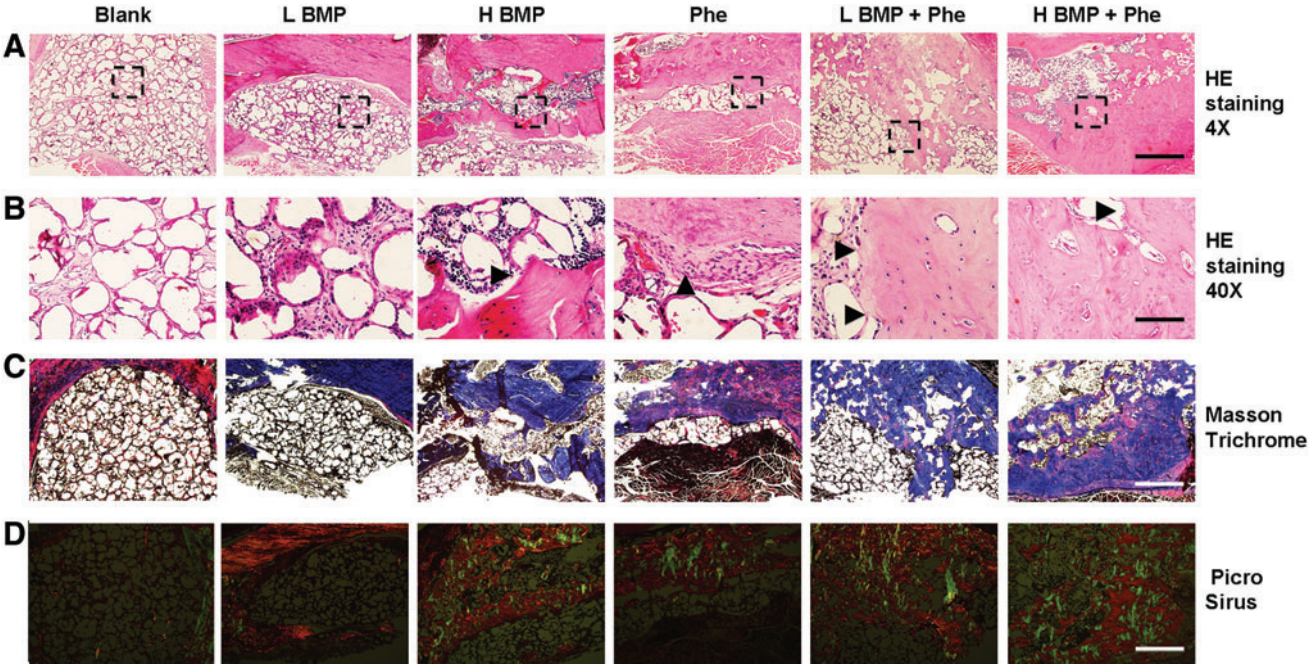

FIG. 6. Histological analysis of bone regeneration in mandibular defects treated with BMP-2 and phenamil. **(A, B)** Histological staining of mandibular defects treated with Ap-PLGA scaffolds loaded with BMP-2 and phenamil at 8 weeks postoperatively. *Arrowhead* indicates new bone tissues. Area within the *black box* indicates the high magnification of image below. *Black arrowhead* indicates new bone formation. Images were taken at 4× magnification for *top image* and 40× magnification for *bottom image*. *Top* scale bar = 500 μm, *Bottom* scale bar = 50 μm. **(C)** Masson's trichrome staining. Images were taken at 4× magnification, scale bar = 500 μm. **(D)** Sirius red staining at polarized light. Images were taken at 4× magnification. Scale bar = 500 μm. Color images available online at www.liebertpub.com/tea

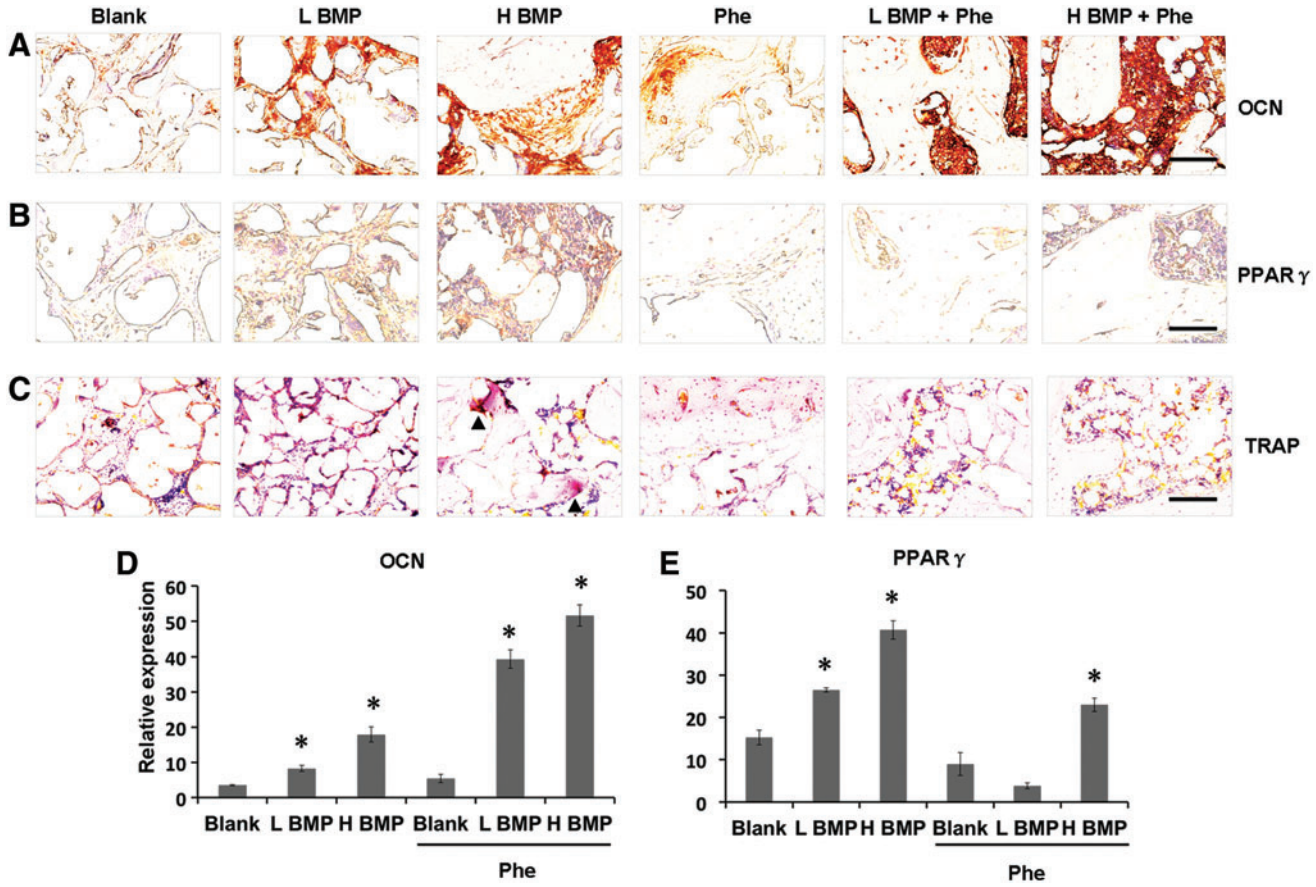

FIG. 7. Histological and immunohistochemical analysis of bone regeneration in mandibular defects treated with BMP-2 and phenamil. **(A, B)** Immunohistochemical staining for OCN and PPARγ expression. **(C)** TRAP staining for detecting osteoclast cells in mandibular defect. *Black arrowhead* indicates osteoclast cell. **(D, E)** Semiquantitative analysis of OCN and PPARγ staining using ImageJ software. Images were taken at 40× magnification. Scale bar = 50 μm. Data presented as mean ± SD ($n = 3$/group), $*p < 0.05$. TRAP, tartrate-resistant acid phosphatase. Color images available online at www.liebertpub.com/tea

healing with over 44% increase in BV/TV and 79% increase in bone surface area as grafted in a 5 mm rat mandibular defect at 8 weeks postoperatively. Furthermore, a complementary approach by using BMP-2 2.5 μg + phenamil 300 μM exhibits a synergistic effect on mandibular bone repair resulting in almost complete bone formation. Overall, our study suggested that not only does the exogenous use of BMP-2 coupled with small-molecule phenamil significantly reduce BMP-2 dosage requirement but also it does not compromise the osteogenic efficacy. This combinatorial strategy may be beneficial to the BMP-2-based mandibular bone repair in future.

Another barrier to BMP-mediated bone therapeutics is a dose-dependent activation of PPARγ and adipogenic differentiation that is likely to cause additional undesirable effects such as cyst-like bone void formation.[13,14,38] MSCs can give rise to multiple lineage commitments, including osteoblasts, adipocytes, and chondrocytes. Growing evidences demonstrated that the shift of MSC differentiation to adipogenesis is closely correlated with fatty marrow accretion being linked to the relevant bone loss diseases such as age-related osteoporosis.[39]

Recent increasing attention is toward exploring osteogenic factors that favor osteogenesis over adipogenesis for improved bone repair. In the current work, we demonstrated that phenamil has pro-osteogenic and antiadipogenic effects on hBMSCs, being evident by not just stimulating BMP-2-induced osteogenesis but also by suppressing the elevated adipogenic differentiation caused by high dosing BMP-2. The dual roles of phenamil were further determined in the repair of mandibular defect, where the phenamil-treated defects appear to be no obvious adipogenic expression as measured with immunohistochemical PPARγ staining while showing the increased expression of bone markers observed by OCN staining. The additional adoption of phenamil is therefore suggested to minimize the adverse outcomes of single BMP-2 currently used in the bone defect restoration.

Although significant adverse effects such as adipogenic differentiation with cyst-like bone formation were not detected in our mandibular defect model probably due to relatively low BMP-2 dose applied in this study, further studies will reproduce the adverse outcomes associated with high-dose BMP-2 in our rodent model to investigate whether phenamil can inhibit BMP-2-induced adipogenesis and improve the quality of newly formed bone *in vivo*.

PPARγ is thought to be a key transcriptional regulator to control adipogenic differentiation.[14] A prior study showed that Trb3 inhibits adipocyte differentiation through negatively

regulating the transcriptional activity of PPARγ.[26] Similarly, our studies illustrated that phenamil-treated hBMSCs exhibit an inhibitory effect on the regulation of PPARγ expression *via* induction of Trb3. Also, in consistency with previous findings, Trb3 induction stimulated BMP signaling pathway through inhibition of Smurf-1 and stabilization of Smad 1/5/8. Moreover, these results were consistent in the *in vivo* rat model at as early as 10 days postoperatively.

Of the large number of developed osteoinductive factors, the phenamil was exclusively chosen to cooperate with BMP-2 for bone repair on the basis of its capacity of stimulating Trb3-Smad 1/5/8, which was thought to enable the additive or synergistic effect on BMP signaling when supplemented with BMP-2. Overall, the pro-osteogenic and antiadipogenic effect of phenamil is attributed at least, in part, to the modulation of Trb3, demonstrating that Trb3 may serve as an effective and safe therapeutic target for bone regeneration. Interestingly, it is suggested that Trb3 also attenuates inflammatory cytokine secretion.[40] Further work may be required to investigate whether the use of phenamil impacts BMP-2-mediated inflammation reaction during bone healing.

Therapeutic efficacy of BMP-2 is also affected by delivery kinetics because of its susceptibility in instability and degradation.[41] The current FDA-approved collagen sponge may not provide an appropriate substrate to deliver supraphysiological doses of BMP-2 with poor control over the protein release rate and bioavailability, leading to unwanted bone formation.[41] We previously established a coating process of biomimetic apatite layer on different biomaterial surfaces such as PLGA, tricalcium phosphate, and chitosan, illustrating that the apatite-coated scaffolds not only promote osteogenesis but also control release of loaded BMP-2 with low initial burst.[28,32,42–44]

Besides delivering growth factor BMP-2, apatite-coated PLGA was also revealed to retain a large amount of small-molecule phenamil with high bioactivity and sustained release up to 3 weeks in prior studies.[20] In the present work, apatite-coated PLGA used to deliver both BMP-2 and phenamil demonstrated effective bone regeneration in mandibular defects, further validating the feasibility of the scaffold for the codelivery of small drugs and large proteins. However, we noted that there is still a high initial burst for small-molecule phenamil delivery in the scaffold at the first day maybe owing to its nonspecific adsorbance or small size.[20] Also, the physical adsorption-mediated small-molecule carrier might be easily impacted by scaffold degradation or tissue ingrowth.[45]

An essential work in future study will be to improve the delivery of small osteoinductive molecule by developing a controlled delivery nanocarrier that can be readily integrated with the scaffold. Since many of the adverse effects of BMP-2 are dose related and affected by delivery methods, additional study on the carrier effects will be needed using the current collagen sponge as a standard of comparison to establish the use of BMP-2 and phenamil as an effective and safe therapeutic strategy for bone repair.

In addition, choosing a suitable animal defect model is crucial to tissue engineering strategy for bone repair. Although large animal such as canine is commonly applied to the establishment of segmental mandibular defect,[46,47] a small-animal model with large mandibular discontinuity defects has been investigated in light of consideration for expenditure, surgical technique, and animal care.[48] We recently set up a marginal defect (it simulates human mandibular defect caused by tumor resection or trauma) in rat mandible and determined 5×5 mm as a critical size that would not be spontaneously healed.[49] Likewise, the same size of defect created in rat mandible was carried out in the present study to prove the efficacy of our combination treatment.

Conclusions

In vitro studies indicated that phenamil treatment not only promotes BMP-2-induced osteogenic differentiation of hBMSCs but also suppresses their adipogenic differentiation. Furthermore, mechanistic studies suggested that phenamil mediates its pro-osteogenic and antiadipogenic effect by modulating Trb3 expression, which subsequently enhanced BMP-smad signaling and decreased PPARγ activity. Finally, codelivery of phenamil and BMP-2 from apatite-coated PLGA scaffolds was shown to synergistically coordinate to promote bone repair in a critical-sized rat mandibular defect. These results demonstrate a novel complementary osteoinductive strategy to improve the efficacy and safety of current BMP-2-based therapeutics in bone repair by regulating expression of Trb3.

Acknowledgments

We thank the UCLA pathology laboratory for preparing histological slides. This work was supported by the National Institutes of Health fundings R01 AR060213 and R21 DE021819, the International Association for Dental Research, and the Academy of Osseointegration.

Disclosure Statement

No competing financial interests exist.

References

1. Hadloc, T.A., Vacanti, J.P., and Cheney, M.L. Tissue engineering in facial plastic and reconstructive surgery. Facial Plast Surg **14,** 197, 1998.
2. Guerra, M.F.M., Campo, F.J.R., Gías, L.N., and Pérez, J.S. Rim versus sagittal mandibulectomy for the treatment of squamous cell carcinoma: two types of mandibular preservation. Head Neck **25,** 982, 2003.
3. Urken, M.L., Buchbinder, D., Costantino, P.D., Sinha, U., Okay, D., Lawson, W., and Biller, H.F. Oromandibular reconstruction using microvascular composite flaps: report of 210 cases. Arch Otolaryngol Head Neck Surg **124,** 46, 1998.
4. Suh, J.D., Sercarz, J.A., Abemayor, E., Calcaterra, T.C., Rawnsley, J.D., Alam, D., and Blackwell, K.E. Analysis of outcome and complications in 400 cases of microvascular head and neck reconstruction. Arch Otolaryngol Head Neck Surg **130,** 962, 2004.
5. Wax, M.K., and Rosenthal, E. Etiology of late free flap failures occurring after hospital discharge. Laryngoscope **117,** 1961, 2007.
6. Hidalgo, D.A., and Pusic, A.L. Free-flap mandibular reconstruction: a 10-year follow-up study. Plast Reconstr Surg **110,** 438, 2002.

7. Mikos, A.G., Herring, S.W., Ochareon, P., Elisseeff, J., Lu, H.H., Kandel, R., Schoen, F.J., Toner, M., Mooney, D., Atala, A., Van Dyke, M.E., Kaplan, D., and Vunjak- Novakovic, G. Engineering complex tissues. Tissue Eng **12,** 3307, 2006.
8. Schroeder, J.E., and Mosheiff, R. Tissue engineering approaches for bone repair: concepts and evidence. Injury **42,** 609, 2011.
9. Seto, I., Asahina, I., Oda, M., and Enomoto, S. Reconstruction of the primate mandible with a combination graft of recombinant human bone morphogenetic protein-2 and bone marrow. J Oral Maxillofac Surg **59,** 53, 2001.
10. Reddi, A.H. Role of morphogenetic proteins in skeletal tissue engineering and regeneration. Nat Biotechnol **16,** 247, 1998.
11. Rengachary, S.S. Bone morphogenetic proteins: basic concepts. Neurosurgical Focus **13,** e2, 2002.
12. Carragee, E.J., Hurwitz, E.L., and Weiner, B.K. A critical review of recombinant human bone morphogenetic protein-2 trials in spinal surgery: emerging safety concerns and lessons learned. Spine J **11,** 471, 2001.
13. James, A.W., LaChaud, G., Shen, J., Asatrian, G., Nguyen, V., Zhang, X., Ting, K., and Soo, C. A review of the clinical side effects of bone morphogenetic protein-2. Tissue Eng Part B Rev **22,** 284, 2016.
14. Kang, Q., Song, W.X., Luo, Q., Tang, N., Luo, J., *et al.* A comprehensive analysis of the dual roles of BMPs in regulating adipogenic and osteogenic differentiation of mesenchymal progenitor cells. Stem Cells Dev **18,** 545, 2009.
15. Kim, I.S., Lee, E.N., Cho, T.H., Song, Y.M., Hwang, S.J., Oh, J.H., Park, E.K., Koo, T.Y., and Seo, Y.K. Promising efficacy of *Escherichia coli* recombinant human bone morphogenetic protein-2 in collagen sponge for ectopic and orthotopic bone formation and comparison with mammalian cell recombinant human bone morphogenetic protein-2. Tissue Eng Part A **17,** 337, 2011.
16. Zhang, Q., He, Q.F., Zhang, T.H., Yu, X.L., Liu, Q., and Deng, F.L. Improvement in the delivery system of bone morphogenetic protein-2: a new approach to promote bone formation. Biomed Mater **7,** 045002, 2012.
17. Wu, G., Liu, Y., Iizuka, T., and Hunziker, E.B. The effect of as low mode of BMP-2 delivery on the inflammatory response provoked by bone-defect-filling polymeric scaffolds. Biomaterials **31,** 7485, 2010.
18. James, A.W., Pang, S., Askarinam, A., Corselli, M., Zara, J.N., *et al.* Additive effects of sonic hedgehog and Nell-1 signaling in osteogenic versus adipogenic differentiation of human adipose-derived stromal cells. Stem Cells Dev **21,** 2170, 2012.
19. Marciano, D.P., Kuruvilla, D.S., Boregowda, S.V., Asteian, A., Hughes, T.S., *et al.* Pharmacological repression of PPARγ promotes osteogenesis. Nat Commun **6,** 7443 2015.
20. Fan, J., Im, C.S., Cui, Z.K., Guo, M., Bezouglaia, O., *et al.* Delivery of phenamil enhances BMP-2-induced osteogenic differentiation of adipose-derived stem cells and bone formation in calvarial defects. Tissue Eng Part A **21,** 2053, 2015.
21. Fan. J., Im, C.S., Guo, M., Cui, Z.K., Fartash, A., *et al.* Enhanced osteogenesis of adipose-derived stem cells by regulating bone morphogenetic protein signaling antagonists and agonists. Stem Cells Transl Med **5,** 539, 2016.
22. Lo, K.W., Ashe, K.M., Kan, H.M., and Laurencin, C.T. The role of small molecules in musculoskeletal regeneration. Regen Med **7,** 535, 2012.
23. Park, K.W., Waki, H., Kim, W.K., Davies, B.S., Young, S.G., *et al.* The small molecule phenamil induces osteoblast differentiation and mineralization. *Mol Cell Biol* **29,** 3905, 2009.
24. Lo, K.W., Kan, H.M., and Laurencin, C.T. Short-term administration of small molecule phenamil induced a protracted osteogenic effect on osteoblast-like MC3T3-E1 cells. J Tissue Eng Regen Med **10,** 518, 2013.
25. Kim, J.G., Son, K.M., Park, H.C., Zhu, T., Kwon, J.H., and Yang, H.C. Stimulating effects of quercetin and phenamil on differentiation of human dental pulp cells. Eur J Oral Sci **121,** 559, 2013.
26. Takahashi, Y., Ohoka, N., Hayashi, H., and Sato, R. TRB3 suppresses adipocyte differentiation by negatively regulating PPARgamma transcriptional activity. J Lipid Res **49,** 880, 2008.
27. Bezy, O., Vernochet, C., Gesta, S., Farmer, S.R., and Kahn, C.R. TRB3 blocks adipocyte differentiation through the inhibition of C/EBPbeta transcriptional activity. Mol Cell Biol **27,** 6818, 2007.
28. Chou, Y.F., Dunn, J.C., and Wu, B.M. In vitro response of MC3T3-E1 pre-osteoblasts within three-dimensional apatite-coated PLGA scaffolds. J Biomed Mater Res B Appl Biomater **75,** 81, 2005.
29. Cowan, C.M., Shi, Y.Y., Aalami, O.O., Chou, Y.F., Mari, C., Thomas, R., Quarto, N., Contag, C.H., Wu, B., and Longaker, M.T. Adipose-derived adult stromal cells heal critical-size mouse calvarial defects. Nat Biotechnol **22,** 560, 2004.
30. Aaron, W.J., Theologis, A.A., Brugmann, S.A., Xu, Y., Carrel, A.L., *et al.* Estrogen/estrogen receptor alpha signaling in mouse posterofrontal cranial suture fusion. PLoS One **4,** e7120, 2009.
31. Park, H., Choi, B., Nguyen, J., Fan, J., Shafi, S., *et al.* Anionic carbohydrate-containing chitosan scaffolds for bone regeneration. Carbohydr Polym **97,** 587, 2013.
32. Lee, M., Li, W., Siu, R.K., Whang, J., Zhang, X., *et al.* Biomimetic apatite-coated alginate/chitosan microparticles as osteogenic protein carriers. Biomaterials **30,** 6094, 2009.
33. Fan, J., Park, H., Lee, M.K., Bezouglaia, O., Fartash, A., Kim, J., Aghaloo, T., and Lee, M. Adipose-derived stem cells and BMP-2 delivery in chitosan-based 3D constructs to enhance bone regeneration in a rat mandibular defect model. Tissue Eng Part A **20,** 2169, 2014.
34. Ferretti, C., and Ripamonti, U. Human segmental mandibular defects treated with naturally derived bone morphogenetic proteins. J Craniofac Surg **13,** 434, 2002.
35. Mckay, W.F., Peckham, S.M., and Badura, J.M. A comprehensive clinical review of recombinant human bone morphogenetic protein-2 (INFUSE® Bone Graft). Int Orthop **2,**729, 2007.
36. Arosarena, O., and Collins, W. Comparison of BMP-2 and –4 for rat mandibular bone regeneration at various doses. Orthod Craniofac Res **8,** 267, 2005.
37. Wen, B., Karl, M., Pendrys, D., Shafer, D., Freilich, M., and Kuhn, L. An evaluation of BMP-2 delivery from scaffolds with miniaturized dental implants in a novel rat mandible model. J Biomed Mater Res B Appl Biomater **97,** 315, 2001.
38. Zara, J.N., Siu, R.K., Zhang, X., Shen, J., Ngo, R., *et al.* High doses of bone morphogenetic protein 2 induce structurally abnormal bone and inflammation in vivo. Tissue Eng Part A **17,** 1389, 2011.
39. Astudillo, P., Ríos, S., Pastenes, L., Pino, A.M., and Rodríguez, J.P. Increased adipogenesis of osteoporotic human-

mesenchymal stem cells (MSCs) characterizes by impaired leptin action. J Cell Biochem **103,** 1054, 2008.
40. Borsting, E., Patel, S.V., Declèves, A.E., Lee, S.J., Rahman, Q.M., *et al.* Tribbles homolog 3 attenuates mammalian target of rapamycin complex-2 signaling and inflammation in the diabetic kidney. J Am Soc Nephrol **25,** 2067, 2014.
41. Boerckel, J.D., Kolambkar, Y.M., Dupont, K.M., Uhrig, B.A., Phelps, E.A., *et al.* Effects of protein dose and delivery system on BMP-mediated bone regeneration. Biomaterials **32,** 5241, 2011.
42. Fan, J., Park, H., Tan, S., and Lee, M. Enhanced osteogenesis of adipose derived stem cells with Noggin suppression and delivery of BMP-2. PLoS One **8,** e72474, 2013.
43. Hu, J., Hou, Y., Park, H., and Lee M. Beta-tricalcium phosphate particles as a controlled release carrier of osteogenic proteins for bone tissue engineering. J Biomed Mater Res A **100,** 1680, 2012.
44. Chou, Y.F., Huang, W., Dunn, J.C., Miller, T.A., and Wu, B.M. The effect of biomimetic apatite structure on osteoblast viability, proliferation, and gene expression. Biomaterials **26,** 285, 2015.
45. Pascaud, P., Errassifi, F., Brouillet, F., Sarda, S., Barroug, A., *et al.* Adsorption on apatitic calcium phosphates for drug delivery: interaction with bispho-sphonate molecules. J Mater Sci Mater Med **25,** 2373, 2014.
46. Hussein, K.A., Zakhary, I.E., Elawady, A.R., Emam, H.A., Sharawy, M., *et al.* Difference in soft tissue response between immediate and delayed delivery suggests a new mechanism for recombinant human bone morphogenetic protein 2 action in large segmental bone defects. Tissue Eng Part A **18,** 665, 2012.
47. Jégoux F, Goyenvalle E, Cognet R, Malard, O., Moreau, F., *et al.* Mandibular segmental defect regenerated with macroporous biphasic calcium phosphate, collagen membrane, and bone marrow graft in dogs. Arch Otolaryngol Head Neck Surg **136,** 971, 2010.
48. Schliephake, H., Weich, H.A., Dullin, C., Gruber, R., and Frahse, S. Mandibular bone repair by implantation of rhBMP-2 in a slow release carrier of polylactic acid—an experimental study in rats. Biomaterials **29,** 103, 2008.
49. Sidell, D.R., Aghaloo, T., Tetradis, S., Lee, M., Bezouglaia, O., DeConde, A., and St John, M. Composite mandibulectomy: a novel animal model. Otolaryngol Head Neck Surg **146,** 932, 2012.

Address correspondence to:
Min Lee, PhD
Division of Advanced Prosthodontics
School of Dentistry
University of California, Los Angeles
10833 Le Conte Avenue, CHS 23-088F
Los Angeles, CA 90095-1668

E-mail: leemin@ucla.edu

Tara L. Aghaloo, DDS, MD, PhD
Division of Diagnostic and Surgical Sciences,
School of Dentistry
University of California, Los Angeles
10833 Le Conte Ave, CHS 53-009
Los Angeles, CA 90095-1668

E-mail: taghaloo@dentistry.ucla.edu

Received: July 26, 2016
Accepted: October 12, 2016
Online Publication Date: November 28, 2016